common drug target[27], suggesting that the spindle-associated PARPs are potential cancer drug targets. ☐

Methods

Imaging and antibodies

Cycled *Xenopus* egg extract spindles were assembled as described[12] with or without X-rhodamine-labelled or Alexa-488-labelled tubulin, and isolated through 40% glycerol BRB80. For staining of non-fixed spindles, isolated spindles were processed for immunofluorescence in solutions containing 5% glycerol BRB80. For immunofluorescence and immunoblotting, polyclonal rabbit LP96-10 IgG was purchased from BD Biosciences, polyclonal chicken IgY anti-PAR antibodies from Tulip Biolabs, and monoclonal 10H from Trevigen. All anti-PAR antibodies were pre-adsorbed against BSA transferred to nitrocellulose. LP96-10 Fab fragments were generated using an Immunopure Fab preparation kit (Pierce Biotech). Anti-NuMA, TPX2 and Eg5 polyclonal rabbit antibodies were gifts from A. Groen and D. Miyamoto. Rabbit anti-PARG antibody was obtained from Oncogene Inc. Primary antibodies were directly labelled using Alexa 488 and X-rhodamine NHS esters (Molecular Probes) as per the manufacturer's instructions. Measurements of fluorescence intensity were calculated by background subtraction, then integration of fluorescence. Images were obtained using a Princeton Instruments CCD camera, controlled by Metamorph software (Universal Imaging Corp.). Spinning disk confocal microscopy movies were obtained using a Nikon TE2000U inverted microscope, a Perkin Elmer Ultraview spinning disk confocal head, and a Hamamatsu Orca ER cooled-CCD camera controlled using Metamorph software. Spindle reactions were imaged in open chambers[28], and images obtained every 30 s for 15 min.

Protein purification and biochemistry

Recombinant bovine PARG was expressed and purified as described[29]. For quantification of PAR after PARG treatment, spindles treated with 100 μg ml^{-1} PARG, 100 μg ml^{-1} PARG plus 100 μM ADP-HPD, or untreated spindles were isolated as above and resolved on 8% SDS–PAGE gels, transferred to nitrocellulose, and probed with LP96-10 antibody. CSF was added for comparison.

1. Wittmann, T., Hyman, A. & Desai, A. The spindle: a dynamic assembly of microtubules and motors. *Nature Cell Biol.* **3,** E28–E34 (2001).
2. Smith, S. The world according to PARP. *Trends Biochem. Sci.* **26,** 174–179 (2001).
3. Tulin, A., Stewart, D. & Spradling, A. C. The *Drosophila* heterochromatic gene encoding poly(ADP-ribose) polymerase (PARP) is required to modulate chromatin structure during development. *Genes Dev.* **16,** 2108–2119 (2002).
4. Hatakeyama, K., Nemoto, Y., Ueda, K. & Hayaishi, O. Purification and characterization of poly(ADP-ribose) glycohydrolase. Different modes of action on large and small poly(ADP-ribose). *J. Biol. Chem.* **261,** 14902–14911 (1986).
5. Saxena, A., Saffery, R., Wong, L. H., Kalitsis, P. & Choo, K. H. Centromere proteins Cenpa, Cenpb, and Bub3 interact with poly(ADP-ribose) polymerase-1 protein and are poly(ADP-ribosyl)ated. *J. Biol. Chem.* **277,** 26921–26926 (2002).
6. Kickhoefer, V. A. *et al.* The 193-kD vault protein, VPARP, is a novel poly(ADP-ribose) polymerase. *J. Cell Biol.* **146,** 917–928 (1999).
7. Smith, S. & de Lange, T. Tankyrase promotes telomere elongation in human cells. *Curr. Biol.* **10,** 1299–1302 (2000).
8. Sbodio, J. I. & Chi, N. W. Identification of a tankyrase-binding motif shared by IRAP, TAB182, and human TRF1 but not mouse TRF1. NuMA contains this RXXPDG motif and is a novel tankyrase partner. *J. Biol. Chem.* **277,** 31887–31892 (2002).
9. Bakondi, E. *et al.* Detection of poly(ADP-ribose) polymerase activation in oxidatively stressed cells and tissues using biotinylated NAD substrate. *J. Histochem. Cytochem.* **50,** 91–98 (2002).
10. Earle, E. *et al.* Poly(ADP-ribose) polymerase at active centromeres and neocentromeres at metaphase. *Hum. Mol. Genet.* **9,** 187–194 (2000).
11. Smith, S. & de Lange, T. Cell cycle dependent localization of the telomeric PARP, tankyrase, to nuclear pore complexes and centrosomes. *J. Cell Sci.* **112,** 3649–3656 (1999).
12. Sawin, K. E. & Mitchison, T. J. Mitotic spindle assembly by two different pathways *in vitro*. *J. Cell Biol.* **112,** 925–940 (1991).
13. Slama, J. T. *et al.* Specific inhibition of poly(ADP-ribose) glycohydrolase by adenosine diphosphate (hydroxymethyl)pyrrolidinediol. *J. Med. Chem.* **38,** 389–393 (1995).
14. Wilde, A. & Zheng, Y. Stimulation of microtubule aster formation and spindle assembly by the small GTPase Ran. *Science* **284,** 1359–1362 (1999).
15. Sawin, K. E., LeGuellec, K., Philippe, M. & Mitchison, T. J. Mitotic spindle organization by a plus-end-directed microtubule motor. *Nature* **359,** 540–543 (1992).
16. Compton, D. A., Szilak, I. & Cleveland, D. W. Primary structure of NuMA, an intranuclear protein that defines a novel pathway for segregation of proteins at mitosis. *J. Cell Biol.* **116,** 1395–1408 (1992).
17. Dionne, M. A., Howard, L. & Compton, D. A. NuMA is a component of an insoluble matrix at mitotic spindle poles. *Cell Motil. Cytoskel.* **42,** 189–203 (1999).
18. Olmsted, J. B., Stemple, D. L., Saxton, W. M., Neighbors, B. W. & McIntosh, J. R. Cell cycle-dependent changes in the dynamics of MAP2 and MAP4 in cultured cells. *J. Cell Biol.* **109,** 211–223 (1989).
19. Kapoor, T. M. & Mitchison, T. J. Eg5 is static in bipolar spindles relative to tubulin: evidence for a static spindle matrix. *J. Cell Biol.* **154,** 1125–1133 (2001).
20. Saxton, W. M. *et al.* Tubulin dynamics in cultured mammalian cells. *J. Cell Biol.* **99,** 2175–2186 (1984).
21. Wittmann, T., Wilm, M., Karsenti, E. & Vernos, I. TPX2, A novel *Xenopus* MAP involved in spindle pole organization. *J. Cell Biol.* **149,** 1405–1418 (2000).
22. Poirier, G. G., de Murcia, G., Jongstra-Bilen, J., Niedergang, C. & Mandel, P. Poly(ADP-ribosyl)ation of polynucleosomes causes relaxation of chromatin structure. *Proc. Natl Acad. Sci. USA* **79,** 3423–3427 (1982).
23. Aoufouchi, S. & Shall, S. Regulation by phosphorylation of *Xenopus laevis* poly(ADP-ribose) polymerase enzyme activity during oocyte maturation. *Biochem. J.* **325,** 543–551 (1997).
24. Chi, N. W. & Lodish, H. F. Tankyrase is a golgi-associated mitogen-activated protein kinase substrate that interacts with IRAP in GLUT4 vesicles. *J. Biol. Chem.* **275,** 38437–38444 (2000).
25. Rouleau, M., Aubin, R. A. & Poirier, G. G. Poly(ADP-ribosyl)ated chromatin domains: access granted. *J. Cell Sci.* **117,** 815–825 (2004).
26. Pickett-Heaps, J. D., Forer, A. & Spurck, T. Traction fibre: toward a "tensegral" model of the spindle. *Cell Motil. Cytoskel.* **37,** 1–6 (1997).
27. Troll, W., Garte, S. & Frenkel, K. Suppression of tumor promotion by inhibitors of poly(ADP)ribose formation. *Basic Life Sci.* **52,** 225–232 (1990).
28. Tirnauer, J. S., Salmon, E. D. & Mitchison, T. J. Microtubule plus-end dynamics in *Xenopus* egg extract spindles. *Mol. Biol. Cell* **15,** 1776–1784 (2004).
29. Lin, W., Ame, J. C., Aboul-Ela, N., Jacobson, E. L. & Jacobson, M. K. Isolation and characterization of the cDNA encoding bovine poly(ADP-ribose) glycohydrolase. *J. Biol. Chem.* **272,** 11895–11901 (1997).

··

Structure of an auxilin-bound clathrin coat and its implications for the mechanism of uncoating

Alexander Fotin[1], **Yifan Cheng**[2], **Nikolaus Grigorieff**[3], **Thomas Walz**[2], **Stephen C. Harrison**[4] & **Tomas Kirchhausen**[5]

[1]*Biophysics Graduate Program,* [2]*Department of Cell Biology, Harvard Medical School, 240 Longwood Avenue, Boston, Massachusetts 02115, USA*
[3]*Howard Hughes Medical Institute and Department of Biochemistry, Rosenstiel Basic Medical Sciences Research Center, Brandeis University, 415 South Street, Waltham, Massachusetts 02454, USA*
[4]*Department of Biological Chemistry and Molecular Pharmacology, Harvard Medical School, and Howard Hughes Medical Institute, 250 Longwood Avenue, Boston, Massachusetts 02115, USA*
[5]*Department of Cell Biology and the CBR Institute for Biomedical Research, Harvard Medical School, 200 Longwood Avenue, Boston, Massachusetts 02115, USA*

....

Clathrin-coated pits invaginate from specific membrane compartments and pinch off as coated vesicles. These vesicles then uncoat rapidly once released. The Hsc70 molecular chaperone effects the uncoating reaction, and is guided to appropriate locations on clathrin lattices by the J-domain-containing co-chaperone molecule auxilin[1–4]. This raises the question of how a local event such as ATP hydrolysis by Hsc70 can catalyse a global disassembly. Here, we have used electron cryomicroscopy to determine 12-Å-resolution structures of *in-vitro*-assembled clathrin coats in association with a carboxy-terminal fragment of auxilin that contains both the clathrin-binding region and the J domain. We have located the auxilin fragment by computing differences between these structures and those lacking auxilin (described in an accompanying paper[5]). Auxilin binds within the clathrin lattice near contacts between an inward-projecting C-terminal helical tripod and the crossing of two 'ankle' segments; it also contacts the terminal domain of yet another clathrin 'leg'. It therefore recruits Hsc70 to the neighbourhood of a set of critical interactions. Auxilin binding produces a local

change in heavy-chain contacts, creating a detectable global distortion of the clathrin coat. We propose a mechanism by which local destabilization of the lattice promotes general uncoating.

The clathrin-uncoating activity of Hsc70 was originally identified by biochemical assays *in vitro*[1–3], but convincing demonstration of its *in vivo* function required the characterization of auxilin as its specific co-chaperone[4]. Inactivation of yeast auxilin (Swa2) leads to anomalous accumulation of coated vesicles[6], and RNA interference with nematode auxilin causes similar defects[7]. Mammalian genomes encode two auxilins: auxilin 1 is brain specific[4], whereas auxilin 2 is general[8]. Auxilin 1 is a 910-residue protein with an amino-terminal PTEN-like domain, a central clathrin-binding domain, and a C-terminal Hsc70-binding J domain[4]. Auxilin 2 contains an additional N-terminal kinase domain[9]. Binding to clathrin coats, Hsc70 recruitment and *in vitro* uncoating require only residues 547–910, which comprise the clathrin-binding and J domains[8,10]. The clathrin-binding region of auxilin appears to be largely unstructured in solution[10], but about 25 residues at its C-terminal end contribute two additional helices to the usual three helices of the globular J domain, as revealed by a crystal structure[11] of a fragment comprising residues 810–910 and a solution structure[12] of a slightly larger fragment (residues 776–910). A recent image reconstruction of clathrin coats assembled with full-length auxilin instead of AP-2 adaptor proteins has shown that auxilin forms a shell of density within the coat[13], but the resolution of the map does not allow specific visualization of clathrin–auxilin contacts.

We expressed and purified the 39-kDa C-terminal fragment of auxilin 1 (residues 547–910) comprising the clathrin-binding and J domains. Published studies show that this fragment can direct uncoating by interaction with Hsc70 (ref. 14). We used pre-assembled clathrin coats (containing three-legged clathrin heavy and light chain triskelions) and AP-2 complexes assembled as described in the accompanying paper[5], and obtained site-specific binding of the auxilin fragment by adding increasing amounts of auxilin to coats (Fig. 1). Saturation corresponded to three auxilin molecules bound per clathrin triskelion, in agreement with previous

reports[14,15]. To prepare electron cryomicroscopy samples, we mixed assembled coats with auxilin(547–910) at a molar ratio (clathrin to auxilin) of 1:20 and incubated the mixture for 30 min. To preserve saturation of auxilin-binding sites, we did not remove unbound auxilin(547–910) and carried out the electron microscopy in the presence of an auxilin background. We selected images of hexagonal barrel coats and computed a three-dimensional reconstruction (Fig. 2) at 12 Å resolution as described in Methods.

The map details of auxilin-bound coats resemble closely those of auxilin-free coats[5], but the dimensions of the auxilin-bound D6 barrels (roughly 670×700 Å) are more isometric than those of the unmodified barrels (655×700 Å). Inaccuracy in the determination of electron-microscopic magnification cannot account for the observed effect, as it would produce isotropic differences rather than a difference in axial ratio. The change in shape of the barrel prevented us from computing a difference map directly. We therefore fitted clathrin leg segments into the map, obtained nine averaging transformations as in the accompanying paper[5], and identified density in the averaged map not accounted for by the clathrin model (Fig. 3). In the accompanying paper we describe by the "invariant hub assembly" the tripod and three proximal segments radiating from a vertex, the distal segments (belonging to triskelions centred at nearest-neighbour vertices), and the triangle of ankles (belonging to triskelions centred at second-nearest-neighbour vertices) at the foot of the tripod. Although the proximal, distal and helical tripod parts of the hub assembly superpose well, the orientation of the ankle segment is shifted in the auxilin-bound form, becoming more parallel to the proximal and distal segments and moving the terminal domain radially outward. These local changes must produce the global distortion in axial ratio. There may also be other, more subtle adjustments in clathrin contacts that we are unable to detect at the current level of precision.

Auxilin(547–910) lies close to the site at which the ankle segments cross (Fig. 4), as might be expected from the change in ankle orientation that its binding generates. Density that we ascribe to a
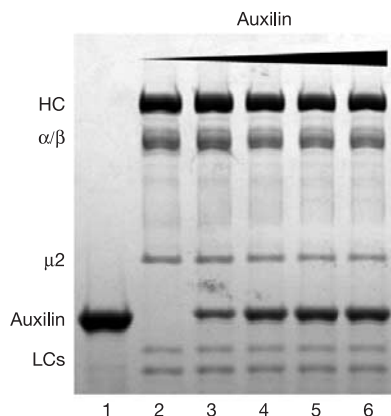

Figure 1 Binding of auxilin(547–910) to clathrin coats. The auxilin fragment was incubated with assembled coats at different molar ratios in reaction buffer for 30 min on ice. The coats were pelleted by high-speed centrifugation for 12 min at 60,000 r.p.m., 4 °C, in a TLA-100 rotor (Beckman). The protein composition of the re-suspended pellets was analysed by SDS–PAGE. Lane 1, auxilin(547–910). Lanes 2–6, pelleted coats after incubation with increasing amounts of auxilin(547–910) using initial molar ratios of auxilin to clathrin heavy chains (HC) as follows: 0:1 (lane 2), 1:1 (lane 3), 3:1 (lane 4), 10:1 (lane 5), 20:1 (lane 6). Saturation achieved by lane 5 corresponds to an estimated 1:1 molar ratio of auxilin(547–910) to clathrin heavy chain. LCs, clathrin light chains LCa and LCb; α/β and μ2, components of the AP-2 complex.
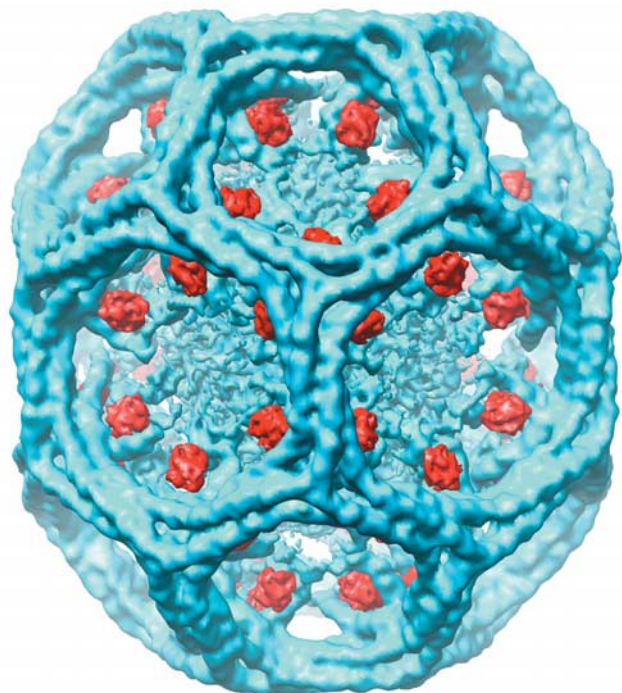

Figure 2 Three-dimensional image reconstruction of a clathrin D6 barrel with bound auxilin(547–910) at 12 Å resolution. The auxilin fragment (identified from local difference maps as described in the text) is rendered in red, whereas the rest of the structure is blue.

single auxilin(547–910) fragment merges (at the resolution of our map) with density from four different clathrin triskelions: a terminal domain, the two chains of the ankle crossing, and (probably) the C-terminal segment that extends from a tripod helix into the ankle-crossing zone (the 'ankle brace'). The putative molecular contacts are consistent with *in vitro* pull-down experiments, showing that auxilin has multiple interactions with different segments of clathrin, including fragments that encompass the terminal domain and the ankle[10].

The structure of the C-terminal 110 residues of bovine auxilin[12] was inserted by inspection into the difference density (Fig. 4). The fragment contains five α-helices, the last three of which are the canonical helices I–III of a J domain. The model of the five helices (residues 800–910) occupies about one-third of the volume that we attribute to the 39-kDa auxilin fragment. It does not seem to participate in any direct interaction with clathrin, in agreement with reported biochemical data showing that the J domain alone does not bind heavy chain[4]. The parts of the J domain believed to associate with Hsc70—the HPD triplet, helix II and the loop connecting helices I and II (ref. 11)—are all exposed on the outward-facing domain surface (Fig. 4c). The structure therefore shows that auxilin will direct Hsc70 to a position beneath the triskelion vertex, adjacent to the clathrin contact that we have proposed determines coat stability[5].

The remaining domain(s) at the N terminus of auxilin, absent from our structure, would probably project inward towards the membrane. If the PTEN-like domain is indeed an active lipid phosphatase, then association of auxilin with a clathrin lattice will place it adjacent to potential substrates.

Proteins in the Hsp70 family, such as *Escherichia coli* DnaK, bind to and release short, exposed hydrophobic segments of polypeptide chain. ATP hydrolysis drives the cycle. The Hsp70 ATPase domain resembles actin; the substrate-binding domain is a molecular clamp with a peptide-binding groove. The coupling of the two domains

has yet to be visualized directly. A J-domain-containing protein recruits ATP-bound Hsp70 to the substrate (for example, an unfolded protein in the best-characterized examples); ATP hydrolysis and dissociation of the J protein leave the Hsp70 molecule clamped to an exposed hydrophobic segment; and binding of a new ATP opens the clamp and restarts the cycle. How can such a simple molecular device couple ATP hydrolysis to disassembly? The structures described here and in the accompanying paper[5] lead to the following suggestions.

Clathrin light chains are not required for uncoating[4]. The best candidate for an unfolded, hydrophobic segment to which Hsc70 can attach is therefore the C terminus (residues 1631–1675) of the heavy chain, which projects into the corners of the triangular structure formed by three crossed ankle regions (Fig. 3a). This is the only part of the heavy chain that does not have a highly organized secondary and tertiary structure[5]. It contains the sequence QLMLT, which shares a noticeable resemblance to the last five residues of the FYQLALT peptide that binds Hsc70 with high affinity and efficiently stimulates its ATPase activity[16]. Moreover, the ankle crossing contacted by this part of the heavy chain is precisely the contact that is perturbed by auxilin binding. Depending on its relative orientation with respect to the ATPase domain, the Hsc70 clamp module could easily reach an exposed C-terminal peptide. The location of auxilin(547–910) and the changes in contacts among nearby clathrin leg segments thus suggest a mechanism by which auxilin could create local strain, release the neighbouring C-terminal segment from its interaction with an ankle, and recruit Hsc70 to clamp and sequester the segment thus exposed.

The change in overall geometry of the clathrin lattice generated by auxilin(547–910) binding also suggests a way in which a perturbation at one vertex could generate distortions at others. A large number of auxilin–Hsc70–C-terminal peptide interactions may not be required to destabilize a coat. If disassembly occurs in the absence of a pool of soluble clathrin that could replace dislocated trimers,
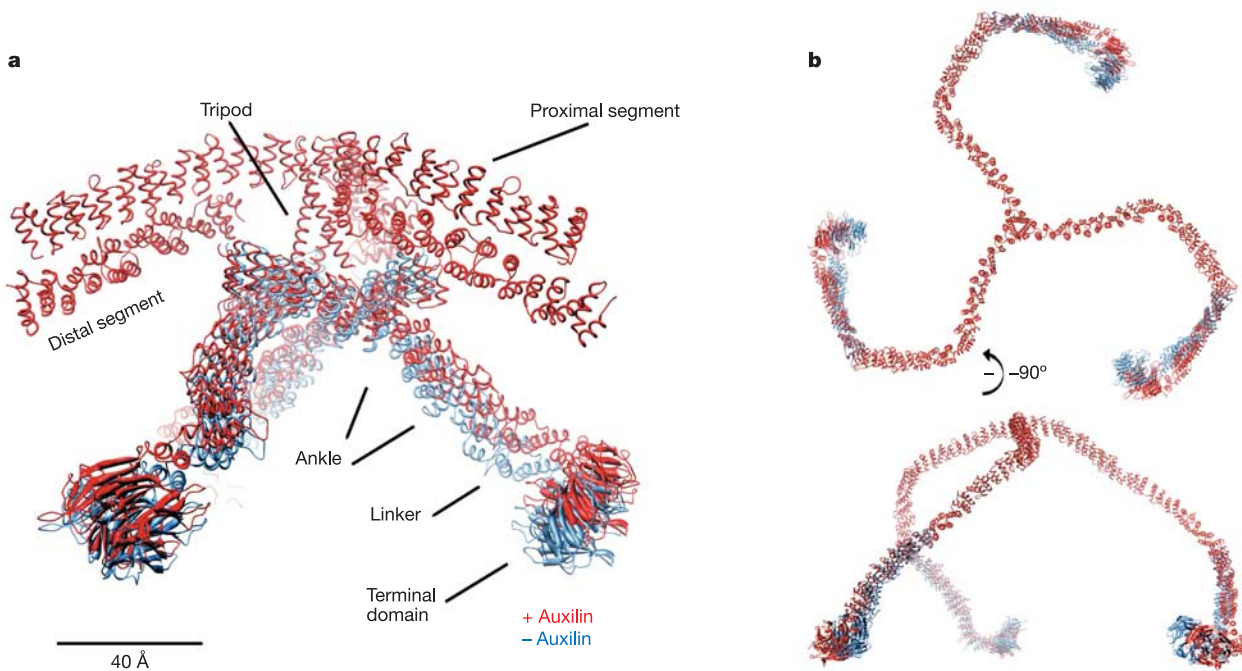

Figure 3 Changes in clathrin heavy-chain contacts produced by auxilin binding.
a, Comparison of the arrangement of clathrin legs in the region around a vertex of the D6 barrel (the "hub assembly", as defined in the accompanying paper[5]). The model from our 7.9 Å resolution analysis of a D6 barrel is in blue; the one obtained by adjusting that model to fit the 12 Å auxilin-bound D6 barrel is in red. The ankle-crossing angles change in such a way that the terminal domains move radially outwards with respect to the outer shell. **b**, Superposition of clathrin triskelions from corresponding locations in the auxilin-bound D6 barrel (red) and the auxilin-free D6 barrel (blue).
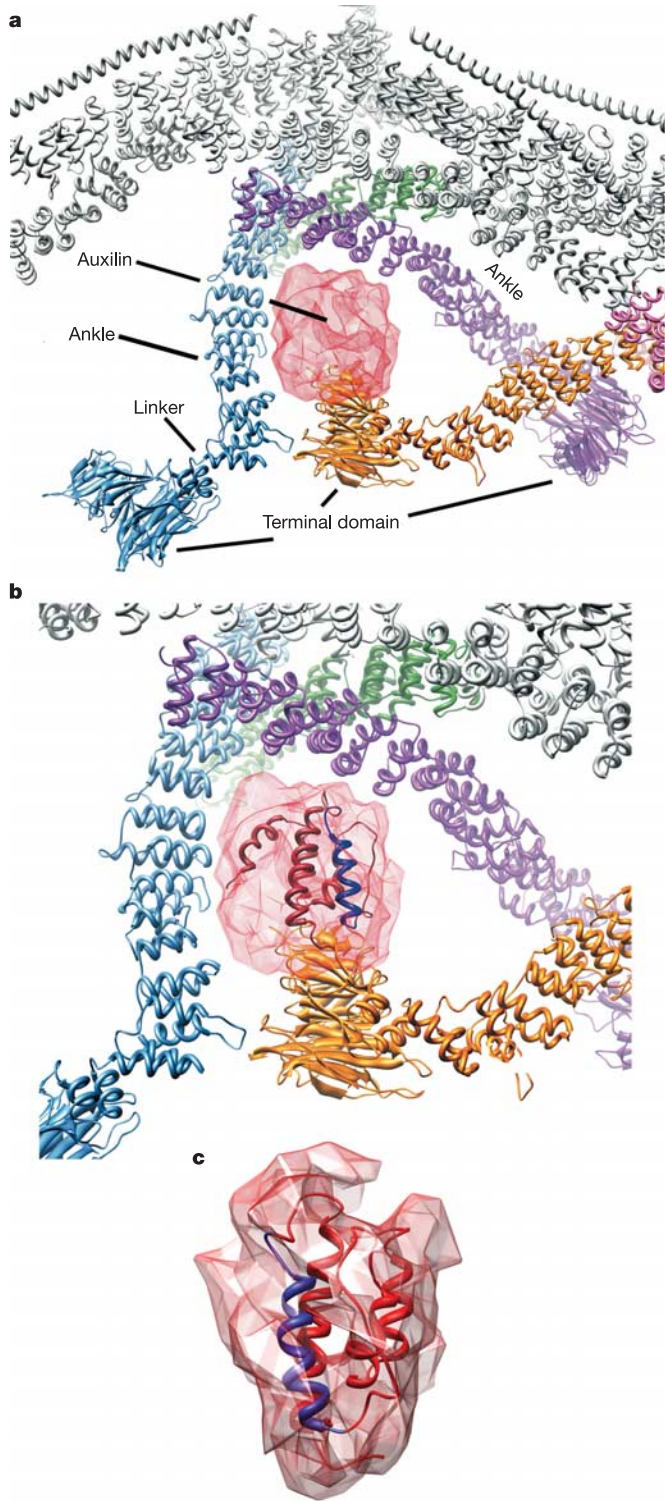
a few clamp-and-sequester events may be sufficient to initiate cooperative uncoating. □

Methods

Specimen preparation

Clathrin coats were assembled from purified clathrin triskelions and AP-2 complex proteins as described in the accompanying paper[5]. DNA encoding full-length bovine auxilin in a pQE-30 vector[17] was provided by E. Ungewickell. The sequence encoding the clathrin-binding region and J domain (amino acid residues 547–910) was amplified from the full-length auxilin DNA by polymerase chain reaction (PCR) with Pfu DNA polymerase (Stratagene) using 5′-GACGTGAGATCTCCGAGTGGACCTACATCC-3′ and 5′-CCTCCGCTCGAGTTAATACAAGGGCTTTTGGCCTTG-3′ as the forward and reverse primers. The PCR product was digested with BglII/XhoI and subcloned into a BamHI/XhoI-digested glutathione S-transferase (GST)-containing pGEX4T-1 vector (Pharmacia). The integrity of the subcloned auxilin DNA fragment was verified by sequencing.

The GST–auxilin(547–910) fusion protein was expressed in E. coli strain BL21. Bacteria were grown at 37 °C to an optical density at 600 nm of 0.6 and then induced with 1 mM IPTG at 25 °C for 3 h. The cells were spun down, re-suspended in 50 ml of PBS, pH 7.4, supplemented with one Complete Protease Inhibitor Cocktail tablet (Roche Applied Science), and lysed by sonication. Cell debris was separated by centrifugation and GST–auxilin(547–910) purified from the supernatant by affinity chromatography on glutathione Sepharose (Pharmacia) according to the manufacturer's instructions. The GST tag was removed by cleaving 1 mg of the Sepharose-bound fusion protein with 1 U of thrombin (Sigma-Aldrich) at 4 °C for 10 h. The cleavage reaction was stopped by addition of PMSF (1 mM final). GST-free auxilin(547–910) was further purified by gel filtration chromatography using a Superose 12 column (Amersham Biosciences) equilibrated with 20 mM HEPES, pH 7.0, 2 mM MgCl$_2$, 25 mM KCl, 10 mM (NH4)$_2$SO$_4$. Purified auxilin(547–910) was stored in a frozen state at −80 °C.

Electron cryomicroscopy

To prepare samples for electron microscopy, assembled coats were mixed with auxilin(547–910) in reaction buffer at a molar ratio of 1:20 and incubated on ice for 30 min. To preserve saturation of all auxilin-binding sites, unbound auxilin was not removed. Freezing procedures and electron cryomicroscopy data collection were performed exactly as described in the accompanying paper[5].

We recorded about 300 electron micrographs, which included the data collected from two sample batches prepared on different dates. Image processing was performed only for hexagonal barrel particles. About 6,500 particles were picked from the selected 190 high-quality micrographs and assembled into the stack. We did not go through the initial stages of particle image classification and class-average-based three-dimensional reconstruction for auxilin-bound particles. Instead, the three-dimensional model of auxilin-free hexagonal barrels (see the accompanying paper[5]) was used as a reference for direct parameter search and refinement in FREALIGN[18].

We first performed FREALIGN refinement in the 800–40 Å resolution range to select the best particles. Images of auxilin-bound clathrin coats had relatively noisier backgrounds when compared with those of auxilin-free complexes mainly due to the presence of unbound auxilin. We therefore used a slightly less stringent criterion for particle selection and included about 900 clathrin coat particles with a PRES value lower than 65° (rather than 62°, as used for auxilin-free samples) in the final refinement procedure. Further refinement of the selected particles produced a 12 Å reconstruction of auxilin-bound clathrin coats as shown in Fig. 2.

1. Schlossman, D. M., Schmid, S. L., Braell, W. A. & Rothman, J. E. An enzyme that removes clathrin coats: Purification of an uncoating ATPase. J. Cell Biol. **99,** 723–733 (1984).
2. Braell, W. A., Schlossman, D. M., Schmid, S. L. & Rothman, J. E. Dissociation of clathrin coats coupled to the hydrolysis of ATP: role of an uncoating ATPase. J. Cell Biol. **99,** 734–741 (1984).
3. Schmid, S. L., Braell, W. A. & Rothman, J. E. ATP catalyzes the sequestration of clathrin during enzymatic uncoating. J. Biol. Chem. **260,** 10057–10062 (1985).
4. Ungewickell, E. et al. Role of auxilin in uncoating clathrin-coated vesicles. Nature **378,** 632–635 (1995).
5. Fotin, A. et al. Molecular model for a complete clathrin lattice from electron cryomicroscopy. Nature doi:10.1038/nature03079 (this issue).
6. Pishvaee, B. et al. A yeast DNA J protein required for uncoating of clathrin-coated vesicles in vivo. Nature Cell Biol. **2,** 958–963 (2000).
7. Greener, T. et al. Caenorhabditis elegans auxilin: a J-domain protein essential for clathrin-mediated endocytosis in vivo. Nature Cell Biol. **3,** 215–219 (2001).
8. Umeda, A., Meyerholz, A. & Ungewickell, E. Identification of the universal cofactor (auxilin 2) in clathrin coat dissociation. Eur. J. Cell Biol. **79,** 336–342 (2000).
9. Ma, Y. et al. Identification of domain required for catalytic activity of auxilin in supporting clathrin uncoating by Hsc70. J. Biol. Chem. **277,** 49267–49274 (2002).
10. Scheele, U., Kalthoff, C. & Ungewickell, E. Multiple interactions of auxilin 1 with clathrin and the AP-2 adaptor complex. J. Biol. Chem. **276,** 36131–36138 (2001).
11. Jiang, J. W. et al. Structure-function analysis of the auxilin J-domain reveals an extended Hsc70 interaction interface. Biochemistry **42,** 5748–5753 (2003).
12. Gruschus, J. M. et al. Structure of the functional fragment of auxilin required for catalytic uncoating of clathrin-coated vesicles. Biochemistry **43,** 3111–3119 (2004).
13. Smith, C. J. et al. Location of auxilin within a clathrin cage. J. Mol. Biol. **336,** 461–471 (2004).

Figure 4 Fit of the auxilin J domain into the difference density. **a**, Auxilin difference density in relation to the hub assembly model. The view is the same as in Fig. 3a. A terminal-domain linker segment projecting towards this hub from another heavy chain centred three vertices away is in gold. The auxilin fragment fits into the intersection of the crossed ankles and also contacts the terminal domain emanating from a different hub. **b**, **c**, Different views showing the fit of the solution structure of the C-terminal, 110-residue fragment of bovine auxilin obtained by NMR[12] into the electron density map. Blue indicates the region of auxilin proposed to contact Hsc70 (ref. 11).

14. Holstein, S. E., Ungewickell, H. & Ungewickell, E. Mechanism of clathrin basket dissociation: separate functions of protein domains of the DnaJ homologue auxilin. *J. Cell Biol.* **135,** 925–937 (1996).
15. Barouch, W., Prasad, K., Greene, L. & Eisenberg, E. Auxilin-induced interaction of the molecular chaperone Hsc70 with clathrin baskets. *Biochemistry* **36,** 4303–4308 (1997).
16. Takenaka, I. M., Leung, S. M., McAndrew, S. J., Brown, J. P. & Hightower, L. E. Hsc70-binding peptides selected from a phage display peptide library that resemble organellar targeting sequences. *J. Biol. Chem.* **270,** 19839–19844 (1995).
17. Schroder, S. *et al.* Primary structure of the neuronal clathrin-associated protein auxilin and its expression in bacteria. *Eur. J. Biochem.* **228,** 297–304 (1995).
18. Grigorieff, N. Three-dimensional structure of bovine NADH:ubiquinone oxidoreductase (complex I) at 22 Å in ice. *J. Mol. Biol.* **277,** 1033–1046 (1998).

carries a side mutation(s) that profoundly impairs chemotaxis to the odorant isoamyl alcohol, indicating that we need to re-evaluate our conclusion from the results shown in Fig. 1 that the *let-60(n1046gf)* mutant has a reduced efficiency of odorant chemotaxis. We outcrossed MT2124 to the wild-type N2 and obtained two *let-60(n1046gf)* strains, JN130 and JN131. We also outcrossed the MT4866 strain, the *let-60(n2021lf)* strain used in the study, and obtained the JN148 strain. All the outcrossed strains show reduced chemotaxis to the two odorants tested, isoamyl alcohol and diacetyl, at low odorant concentrations (T.H. and Y.I., unpublished results). The chemotaxis defects are comparable in extent to, or slightly weaker than, the original MT4866 *let-60(n2021lf)* strain. Our conclusion that both inactivation and hyperactivation of LET-60 Ras cause reduced chemotaxis therefore remains unchanged. However, the result shown in Fig. 1d, which suggested that *ksr-1(lf)*, *mek-2(lf)* and *mpk-1(lf)* suppress *let-60(n1046gf)*, is no longer valid because outcrossed *let-60(n1046gf)* strains do not show chemotaxis defects at the odorant concentration used in Fig. 1d (1×10^{-3} dilution of isoamyl alcohol). □

··

corrigenda

The Ras–MAPK pathway is important for olfaction in *Caenorhabditis elegans*

Takaaki Hirotsu, Satoshi Saeki, Masayuki Yamamoto & Yuichi Iino

Nature **404,** 289–293 (2000).

In this Letter, we used strain MT2124, the standard *let-60(n1046gf)* strain maintained in the *Caenorhabditis* Genetics Center, for odour-chemotaxis assays. However, we have found that this strain

Contrasting origins of the upper mantle revealed by hafnium and lead isotopes from the Southeast Indian Ridge

Barry B. Hanan, Janne Blichert-Toft, Douglas G. Pyle & David M. Christie

Nature **432,** 91–94 (2004).

In this Letter, the quantity ε_{Hf} in Fig. 3 and its legend should read $\Delta\varepsilon_{Hf}$, which is the change in hafnium isotopic composition relative to the ε_{Nd}–ε_{Hf} mantle array. □